Electronic Supplementary Information for: Ultrafast $Z \rightarrow E$ Photoisomerisation of Structurally Modified Furylfulgides

Falk Renth,[1,*] Ron Siewertsen,[1] Frank Strübe,[2] Jochen Mattay,[2] and Friedrich Temps[1,*]

[1] *Institut für Physikalische Chemie, Christian-Albrechts-Universität zu Kiel, Olshausenstr. 40, D-24098 Kiel, Germany*

[2] *Organische Chemie I, Fakultät für Chemie, Universität Bielefeld, Postfach 100131, D-33501 Bielefeld, Germany*

[*] Authors to whom correspondence should be addressed; renth@phc.uni-kiel.de, temps@phc.uni-kiel.de

1. Solvent contributions and time-zero correction

In addition to the molecular contributions of interest, the recorded transient absorption data at short delay times feature unwanted signal contributions from cross phase modulation (XPM), stimulated Raman amplification (SRA), its time analog impulsive stimulated Raman scattering, and two-photon absorption.[1–4] In order to subtract these contributions from the sample data and to characterise the chirp of the supercontinuum probe light, an independent transient absorption experiment with pure solvent under otherwise identical experimental conditions was performed. The center of the XPM-envelope was determined for the solvent data at up to 28 probe wavelengths, and the resulting coordinate set was fitted with a fifth-order polynomial. This function that describes the experimental time-zero t_0 was then employed for time-zero correction of the raw sample and solvent data matrices, using linear interpolation where necessary. To obtain the two-dimensional transient absorption maps (see Fig. 3 of the paper), the time-corrected solvent data were scaled by a suitable factor taking into account the pump pulse absorption and subtracted from the time-corrected sample data. For the sample time profiles at fixed wavelengths (e.g., Figures S1 and S2), the XPM was parametrized by fitting the corresponding solvent time profile with a sum of Gaussians before subtraction. In the subsequent quantitative analysis of the sample time profiles, t_0 was treated as a fit parameter. Typical deviations between the values of t_0 determined from the solvent XPM and as parameter in the fits were in the range of only a few femtoseconds.

2. Non-linear least squares fit

2.1. Fit model

The standard way to describe the transient absorption time profiles at fixed probe wavelengths $\Delta OD_\lambda(t)$ is a fit with a sum of exponential decays with amplitude a_i and decay constants τ_i, multiplied by the Heaviside step function $\mathcal{H}(t-t_0)$ centered at t_0 and convolved with the instrument response function (IRF) in order to take into account the onset and experimental time resolution,[5]

$$\Delta OD_\lambda(t; t_0, \{a_i, \tau_i\}) = \sum_{i=1}^{N} a_i \mathcal{H}(t-t_0) \exp\left[-\frac{(t-t_0)}{\tau_i}\right] \otimes \mathrm{IRF}. \qquad \text{(I)}$$

This procedure results in so-called decay associated difference spectra (DADS) given by the amplitudes of the individual exponential decays. However, the DADS are in general not related to distinct contributions by individual molecular species, so that interpretation is not straightforward and amplitude constraints cannot be applied easily to stabilize the fit procedure.

In order to disentangle the contributions belonging to particular molecular species (species associated difference spectra, SADS), the quantitative data description was therefore performed by target analysis.[5] Because each component carries a physical meaning, amplitude constraints or restriction of components to specific wavelength ranges can be used to improve the fits. The target model is based on a simple consecutive scheme:

$$Z \xrightarrow{+h\nu} Z^* \longrightarrow \{E^\#, Z^\#\} \longrightarrow \{E, Z\} \tag{II}$$

Within the scheme, Z^* denotes Z-isomers in the electronically excited state, $E^\#$ and $Z^\#$ are vibrationally hot molecules following isomerisation and internal conversion to the respective electronic ground states, and E and Z refer to thermally equilibrated isomers after vibrational cooling has been completed. The corresponding species-associated dynamic components of the target model are initial ground-state bleach (GSB) of the Z-molecules, excited-state absorption (ESA) and stimulated emission (SE) by the excited-state species Z^*, hot ground state absorption (HGSA) by $E^\#$ and $Z^\#$, and ground state recovery (GSR) due to absorption by the thermally equilibrated E- and Z-isomer reaction products. The $Z \rightarrow E$ photoconversion is reflected by the time-independent permanent absorption changes (PA). It should be noted here that GSR is not an independent component, but is determined by GSB, HGSA and PA (see below). The experimental time resolution is taken into account by convolution with a Gaussian of standard deviation $\sigma_{\mathrm{IRF}} = 40$ fs centered at time zero t_0 as instrument response function (IRF),

$$\mathrm{IRF}(t; t_0, \sigma_{\mathrm{IRF}}) = \frac{1}{\sigma_{\mathrm{IRF}}\sqrt{2\pi}} \exp\left[-\frac{(t-t_0)^2}{2\sigma_{\mathrm{IRF}}^2}\right]. \tag{III}$$

Equations IV - VI define the convoluted step function CS, the convoluted exponential decay CD and the convoluted damped sine function CSin serving as basic functions needed to model the individual transient absorption components and that depend on t_0, σ_{IRF}, the

decay constants τ, damping time τ_d and oscillation period T as parameters:

$$\mathrm{CS}(t;t_0,\sigma_{\mathrm{IRF}}) = \frac{1}{2}\mathrm{erfc}\left[-\frac{t-t_0}{\sqrt{2}\sigma_{\mathrm{IRF}}}\right] \tag{IV}$$

$$\mathrm{CD}(t;t_0,\tau,\sigma_{\mathrm{IRF}}) = \frac{1}{2}\exp\left[\frac{\sigma_{\mathrm{IRF}}^2}{2\tau^2}-\frac{t-t_0}{\tau}\right]\times\mathrm{erfc}\left[\frac{\sigma_{\mathrm{IRF}}^2/\tau-(t-t_0)}{\sigma_{\mathrm{IRF}}\sqrt{2}}\right] \tag{V}$$

$$\mathrm{CSin}(t;t_0,T,\tau_d,\sigma_{\mathrm{IRF}}) = \frac{i}{2}\left[\mathrm{CD}(t;t_0,\frac{1}{1/\tau_d+i2\pi/T},\sigma_{\mathrm{IRF}})-\mathrm{CD}(t;t_0,\frac{1}{1/\tau_d-i2\pi/T},\sigma_{\mathrm{IRF}})\right] \tag{VI}$$

In accordance with the approach of Ref. 2, respective time delays Δt were used as additional parameters to model temporally delayed components. GSB was described by a step function centered at t_0, SE and ESA were described by single exponentials with respective time constants of τ_{SE} and τ_1. The slightly delayed onset of ESA in the UV spectral region and of SE at the very longest probe wavelengths ($\lambda_{\mathrm{probe}} > 500$ nm) was taken into account by time delays Δt_{ESA} and Δt_{SE}. HGSA was modelled by a biexponential decay with time constants τ_2 and τ_3 representing the fast initial spectral dynamics and the slower vibrational cooling. The temporal delay parameter Δt_{HGSA} accounted for the delayed impulsive rise of HGSA. GSR was modelled as an exponential rise with a rise time equal to τ_3, and an exponentially damped CSin function with a dampening time τ_d and a period T_{OSC} was used to describe the weak damped HGSA oscillations in the wings of the ground state absorption band. Both components were time-shifted by Δt_{HGSA}, too. Slightly larger values σ_{ESA} and σ_{HGSA} compared to the experimental time resolution σ_{IRF} were used to model the rise behavior (slower than limited by the IRF) of ESA in the UV spectral range and of HGSA. For GSB, SE, and ESA at visible probe wavelengths, σ_{IRF} was kept unchanged. The resulting expressions including amplitude parameters are:

$$\mathrm{GSB}(t) = a_{\mathrm{GSB}}\mathrm{CS}(t;t_0,\sigma_{\mathrm{IRF}}) \tag{VII}$$

$$\mathrm{SE}(t) = a_{\mathrm{SE}}\mathrm{CD}(t;t_0+\Delta t_{\mathrm{SE}},\tau_{\mathrm{SE}},\sigma_{\mathrm{IRF}}) \tag{VIII}$$

$$\mathrm{ESA}(t) = a_1\mathrm{CD}(t;t_0,\tau_1,\sigma_{\mathrm{IRF}}) \quad (\text{at } \lambda_{\mathrm{probe}} \gtrsim 400\mathrm{nm}) \tag{IX}$$

$$\mathrm{ESA}(t) = a_1\mathrm{CD}(t;t_0+\Delta t_{\mathrm{ESA}},\tau_1,\sigma_{\mathrm{ESA}}) \quad (\text{at } \lambda_{\mathrm{probe}} \lesssim 400\mathrm{nm}) \tag{X}$$

$$\mathrm{HGSA}(t) = a_2\mathrm{CD}(t;t_0+\Delta t_{\mathrm{HGSA}},\tau_2,\sigma_{\mathrm{HGSA}}) + a_3\mathrm{CD}(t;t_0+\Delta t_{\mathrm{HGSA}},\tau_3,\sigma_{\mathrm{HGSA}}) \tag{XI}$$

$$\mathrm{OSC}(t) = a_{\mathrm{OSC}}\mathrm{CSin}(t;t_0+\Delta t_{\mathrm{HGSA}},T_{\mathrm{OSC}},\tau_d,\sigma_{\mathrm{HGSA}}) \tag{XII}$$

$$\mathrm{GSR}(t) = (a_{\mathrm{PA}}-a_{\mathrm{GSB}})\big[\mathrm{CS}(t;t_0+\Delta t_{\mathrm{HGSA}},\sigma_{\mathrm{HGSA}})-\mathrm{CD}(t;t_0+\Delta t_{\mathrm{HGSA}},\tau_3,\sigma_{\mathrm{HGSA}})\big] \tag{XIII}$$

2.2. Fit procedure

For a reliable quantitative description of the data, simultaneous non-linear least-squares fitting of multiple time profiles at fixed probe wavelengths $\Delta OD_\lambda(t)$ was performed. In order to break up parameter correlation, the number of temporal fit parameters was kept to a minimum by taking τ_1, Δt_{HGSA}, σ_{HGSA}, τ_d and T_{osc}, as well as σ_{IRF} as global parameters. To reduce the number of amplitude parameters in the target model, the amplitudes of the permanent transient absorption changes at large delays, $a_{\mathrm{PA}} = \Delta\mathrm{OD}(\lambda, t \to \infty)$, were obtained by fitting with the difference of the static E- and Z-isomer UV/VIS spectra weighted by a positive factor w_{ZE},

$$\begin{aligned} a_{\mathrm{PA}} &= w_{\mathrm{ZE}} \left(\varepsilon_{\mathrm{E}}(\lambda) - \varepsilon_{\mathrm{Z}}(\lambda)\right) \\ &= \Delta c_{\mathrm{E}} \varepsilon_{\mathrm{E}}(\lambda) + \Delta c_{\mathrm{Z}} \varepsilon_{\mathrm{Z}}(\lambda). \end{aligned} \tag{XIV}$$

The second line of Eq. XIV is the Beer-Lambert law for $\Delta\mathrm{OD}(\lambda, t \to \infty)$ expressed via the concentration changes Δc_{Z} and Δc_{E} (negative for the Z-isomer reactants, positive for the E-isomer products). Therefore $\Delta c_{\mathrm{Z}} = -w_{\mathrm{ZE}}$, and the concentration of the photo-excited species c^*_{Z} can be written as

$$c^*_{\mathrm{Z}} = -\Delta c_{\mathrm{Z}} / \phi_{\mathrm{ZE}} = w_{\mathrm{ZE}} / \phi_{\mathrm{ZE}}, \tag{XV}$$

so that the amplitude of the initial bleach a_{GSB} is given by

$$a_{\mathrm{GSB}} = -c^*_{\mathrm{Z}} \varepsilon_{\mathrm{Z}} = -w_{\mathrm{ZE}} \varepsilon_{\mathrm{Z}} / \phi_{\mathrm{ZE}}. \tag{XVI}$$

The GSB amplitudes are thus entirely determined by the isomerisation quantum yield (and the known Z-isomer UV/VIS spectrum). For Z-MeF and Z-MeBF, the values of ϕ_{ZE} are known ($\phi_{\mathrm{ZE}} = 0.11$),[6,7] so that there is no free parameter left over. In case of Z-iPrF and Z-7rF, ϕ_{ZE} remains as a single global fit parameter. Since GSR is just the difference between GSB and PA, this is the same for the amplitudes of GSR, a_{GSR}. Equations XIV and XVI further imply that the PA, GSB and GSR components can be omitted from the fit outside the relevant wavelength ranges given by the stativ UV/VIS absorption spectra of the Z- and E-isomers. Furthermore, the amplitudes of ESA, HGSA and GSR were constrained to non-negative values, GSB and SE were set to be purely negative. Sensible starting values for the global non-linear fits were explored by single-wavelength fitting. Overall, this procedure

gave a significant improvement in fitting reliability for the selected target model and yielded a quantitative description of the data with low residuals.

3. Adequacy of the target model

Explicit comparison of non-linear least-squares fits obtained by the target model (Eqs. VII - XIII) with alternative fit descriptions is used to confirm (i) the adequacy of additional time delays to describe the impulsive rise of HGSA, and (ii) the validity of the SE component at large probe wavelengths. Figure S1 shows the results of non-linear least-squares fits of the transient absorption time profile for Z-MeBF at $\lambda_{\mathrm{probe}} = 400$ nm by the target model and by a fit with a sum of four exponentials according to Eq. I, i.e. without time delays. For the latter, one decay constant (τ_4) was set to 10^6 to mimick a step function.

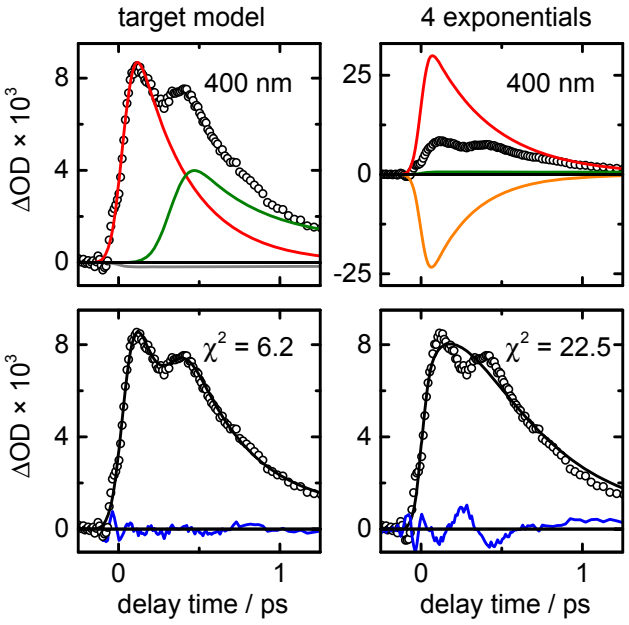

Fig. S1: Comparison of fit results for the time profile of Z-MeBF at $\lambda_{\mathrm{probe}} = 400$ nm. Left: Fit by the target model. Right: Fit by a sum of four exponentials. Data points are represented by open circles. Top row: Individual fit components (coloured lines). Bottom row: Data fits and residuals (black and blue lines) with sum of squared errors χ^2.

The failure of the exponential fit to describe the delayed implusive rise of the HGSA is clearly evidenced by its much larger sum of squared errors compared to the target model fit, and by the systematic deviations that show up in its residuals. Increasing the number of ex-

ponentials does not remove the systematic deviations and gives only marginal improvement. Furthermore, the amplitudes of the two fastest-decaying exponentials (red and orange lines in Fig. S1) for the exponential fit are artificially high as a result of strong correlation. In contrast, the target model provides an excellent fit without systematic deviations, demonstrating the suitability of a time delay to describe the delayed onset of HGSA.

Figure S2 compares the non-linear least-squares fits of the transient absorption time profiles for Z-7rF at $\lambda_{\mathrm{probe}} = 475$, 500 and 525 nm by the target model, i.e. with a negative (SE) component, and by corresponding fits that lack any negative component, but allow for an increased IRF standard deviation σ_{IRF}.

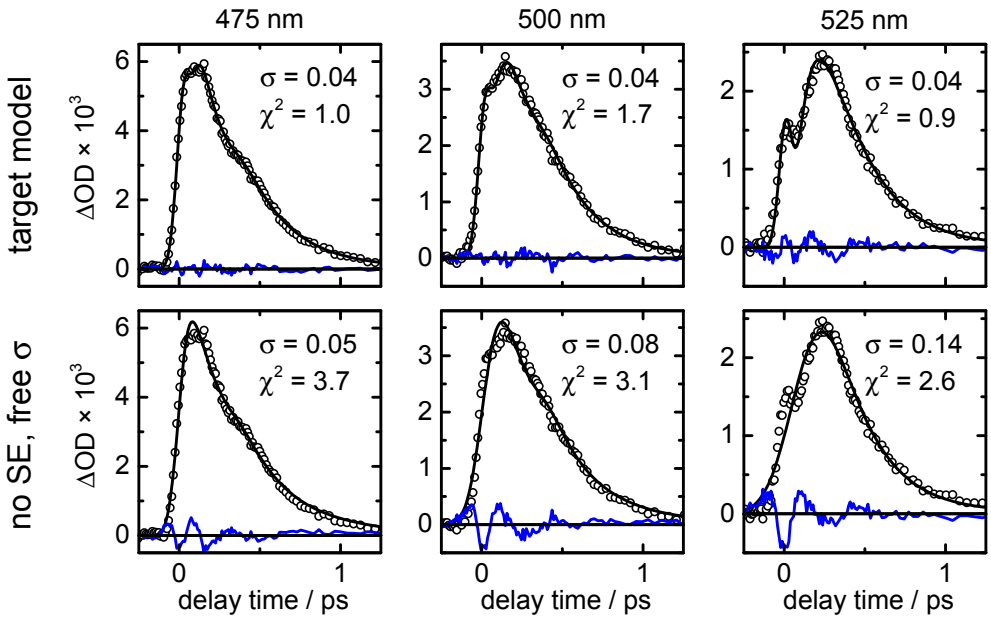

Fig. S2: Comparison of nonlinear least-squares fit results for the time profiles of Z-7rF at $\lambda_{\mathrm{probe}} =$ 475, 500 and 525 nm. Data points are represented by open circles, data fits and the related residuals by black and blue lines, respectively. Top row: fits by the target model with negative SE component. Bottom row: Fit model without negative component, but increased σ_{IRF}. The respective sums of squared errors χ^2 and values of σ_{IRF} are indicated in the legends.

The transient absorption time profiles feature a cropped appearance of the maximum at short delay times developing into a discontinuous rise for $\lambda_{\mathrm{probe}} = 525$ nm, which can be interpreted as an indication of a fast-decaying and probably red-shifting negative (SE) component. The residuals and quoted sum of errors show clearly that a fit description without such a negative (SE) component does not describe the time profiles well, but leads

to increasing systematic deviations at larger probe wavelengths. Concurrently, a rise of the fitted σ_{IRF} happens to values up to $\sigma_{\mathrm{IRF}} = 0.14$. Considering that this corresponds to more than three times the experimental time resolution, the relevance of the fits lacking a negative component is doubtful. In contrast, the fit by the target model is excellent for the lower two probe wavelengths and captures the essential features of the time profile at $\lambda_{\mathrm{probe}} = 525$ nm correctly. The use of a negative SE component in the target model at longer probe wavelengths seems therefore fully justified, even though SE does not show up directly in the form of negative signals but is hidden underneath the larger positive ESA contribution.

---

[1] R. Berera, R. van Grondelle and J. T. M. Kennis, *Photosynth. Res.*, 2009, **101**, 105–118.

[2] J. Briand, O. Bräm, J. Réhault, J. Léonard, A. Cannizzo, M. Chergui, V. Zanirato, M. Olivucci, J. Helbing and S. Haacke, *Phys. Chem. Chem. Phys.*, 2010, **12**, 3178–3187.

[3] S. A. Kovalenko, A. L. Dobryakov, J. Ruthmann and N. P. Ernsting, *Phys. Rev. A*, 1999, **59**, 2369–2384.

[4] U. Megerle, I. Pugliesi, C. Schriever, C. F. Sailer and E. Riedle, *Appl. Phys. B*, 2009, **96**, 215–231.

[5] I. H. M. van Stokkum, D. H. Larsen and R. van Grondelle, *Biochim. Biophys. Acta*, 2004, **1657**, 82104.

[6] F. Strübe, R. Siewertsen, F. D. Sönnichsen, F. Renth, F. Temps and J. Mattay, *Eur. J. Org. Chem.*, 2011, 1947–1955.

[7] E. Uhlmann and G. Gauglitz, *J. Photochem. Photobiol. A*, 1996, **98**, 45–49.